Anal. Chem. **2002,** *74,* 5717−5725

Optimization of the Geometry and Porosity of Microelectrode Arrays for Sensor Design

Mairi E. Sandison, Natalie Anicet, Andrew Glidle, and Jonathan M. Cooper*

Department of Electronics and Electrical Engineering, University of Glasgow, Glasgow, G12 8LT, U.K.

This paper describes the systematic investigation of a range of microelectrode arrays with varying dimensions fabricated by standard photolithographic and reactive-ion etching techniques. As expected from theory, the electrochemical behavior of microelectrode arrays with a constant individual diameter varied strongly with center-to-center spacing, the larger the spacing the more sigmoidal the recorded voltammogram. Furthermore, the behavior of arrays with a constant relative center-to-center spacing is shown to vary with individual electrode diameter, the arrays with the smallest electrodes producing strongly peaked voltammograms. Peak current densities and signal-to-noise ratios were also obtained for a variety of array geometries, and the use of electrodeposited platinum black electrodes was investigated. To demonstrate one advantage of using a loosely packed microelectrode array in electroanalysis, a ferrocene-mediated enzyme-linked assay involving the biocatalytic reduction of H_2O_2 was investigated. Results showed an improved temporal response, with current−time transients reaching a steady-state response more quickly using arrays with increased center−center spacings.

In recent years, thin-film microfabrication technologies developed by the semiconductor industry have increasingly been employed to produce microelectrode structures. Today, microelectrodes are recognized as an important analytical tool, with high sensitivities, fast response times, and well-defined, reproducible geometries.[1] Numerous electroanalytical techniques may be performed using microelectrode structures, many of which exhibit significantly improved Faradic-to-capacitive current ratios and substantially reduced ohmic potential drops when compared to that of conventional macroelectrodes.[2] For example, reliable cyclic voltammetry may be performed with extremely high scan rates and measurements in poorly conducting solutions may be readily obtained.

One of the most significant advantages of microelectrodes is that the steady-state current, which is reached extremely quickly after the application of a potential step, is essentially convection independent.[3,4] Furthermore, when compared to their macroscopic counterparts, thin-film microelectrodes generate greatly increased current densities, as diffusion fields, which are essentially linear for macroscopic electrodes, become increasingly nonlinear with decreasing electrode size.[5,6] In the case of a planar microdisk electrode, the diffusion field of an electroactive species toward the electrode surface tends toward a hemispherical profile.

The Cottrell equation is derived by solving Fick's second law of diffusion[7] by assuming semi-infinite, linear diffusion to a horizontal plane and therefore cannot be used to describe microelectrode behavior. Instead, a time-independent correction term must be incorporated to express the current profile of a microelectrode after the application of a potential step. The resulting equation for a single, inlaid, microdisk electrode yields a limiting current, i_L, that is time independent and varies with radius, r, rather than area.[6] Hence, microelectrode current density varies inversely with r and thus the smaller the microelectrode, the greater the current density.

If a microelectrode is recessed, as is typical for a thin-film microelectrode structure (Figure 1a), the diffusion profile is different from that of an inlaid microelectrode and mass transport to the electrode surface is reduced by an amount dependent upon the height of the recess. For a single, recessed microdisk electrode, where n is the number of electrons exchanged, F the Faraday constant, D the diffusion coefficient of the electroactive species, c_∞ its concentration in the bulk solution, and h the height of the recess, eq 1 describes i_L accordingly[8]

$$i_L = \pi r^2 nFD\frac{c_\infty}{r + h} \qquad (1)$$

Although microelectrodes yield extremely large current densities, they generate very small currents. Thus, microelectrode arrays have been used to produce sensors with both high current densities and satisfactory output signals.[9−12] However, the center−

* Corresponding author: (e-mail) jmcooper@elec.gla.ac.uk; (fax) +44 141 330 6010.

(1) Feeney, R.; Kounaves, S. P. *Electroanalysis* **1999**, *12* (10), 677−684.
(2) Štulík, K.; Amatore, C.; Holub, K.; Mare_ek, V.; Kutner, W. *Pure Appl. Chem.* **2000**, *72* (8), 1483−1492.
(3) Morf, W. E. *Anal. Chim. Acta* **1996**, *330* (2−3), 139−149.
(4) Morf, W. E.; de Rooij, N. F. *Sens. Actuators, B* **1997**, *44*, 538−541.
(5) Aoki, K. *Electroanalysis* **1993**, *5* (8), 627−639.
(6) Heinze, J. *Angew. Chem., Int. Ed.* **1991**, *32* (9), 1268−1288.
(7) Bard, A. J.; Faulkner, L. R. *Electrochemical methods: fundamentals and applications*, 2nd ed.; John Wiley & Sons Inc.: New York, 2001.
(8) Lenigk, R.; Zhu, H. X.; Lo, T. C.; Renneberg, R. *Fresenius J. Anal. Chem.* **1999**, *364* (1−2), 66−71.
(9) Belmont-Hebert, C.; Tercier, M. L.; Buffle, J.; Fiaccabrino, G. C.; de Rooij, N. F.; Koudelka-Hep, M. *Anal. Chem.* **1998**, *70*, (14), 2949−2956.
(10) Feeney, R.; Kounaves, S. P. *Anal. Chem.* **2000**, *72* (10), 2222−2228.
(11) Schwake, A.; Ross, B.; Cammann, K. *Sens. Actuators, B* **1998**, *46*, 242−248.
(12) Wittkampf, M.; Chemnitius, G. C.; Cammann, K.; Rospert, M.; Mokwa, W. *Sens. Actuators, B* **1997,** *43*, 40−44.

10.1021/ac025649w CCC: $22.00
Published on Web 10/16/2002

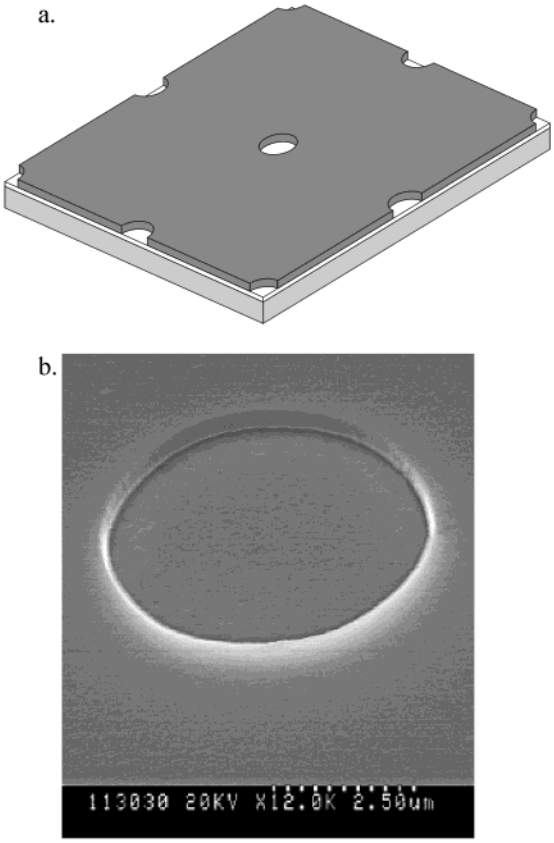

Figure 1. (a) Cross section schematic of a microfabricated electrode array (the light gray layer represents the substrate, the white layer the metal, and the dark gray layer the insulating material) (b) SEM of a recessed gold electrode (the electrode radius is 2.5 μm and the depth of recess is 500 nm).

center spacing, *d*, between individual microelectrodes is crucial and significantly effects electrochemical behavior. If the interelectrode distance is sufficiently large, the microelectrode array will behave as multiple single electrodes in parallel and produce a limiting current of $i_L m$, where *m* is the number of electrodes in the array. In contrast, when very short interelectrode distances are employed, the advantages of using microelectrodes will be greatly reduced, as the individual diffusion fields will merge to form a linear diffusion layer.[1,13] Microelectrode arrays with intermediate spacings will exhibit a mixed diffusion profile, where diffusion is assumed to be radial in the regions bordering a microelectrode but planar further away from the active surfaces.[3]

The electrochemical behavior of different arrays with the same relative interelectrode spacing, *d*/*r*, is affected by various parameters including *r* and, for voltammetry experiments, the scan rate.[14] It should also be noted that, although deep recesses may reduce the benefits of employing microelectrodes, it has been shown that the overlap between the diffusion fields of the individual electrodes will occur to a lesser degree for recessed electrodes.[15]

Electroplating microelectrodes with mesoporous "platinum black" will have the effect of enhancing the electrochemical signal[16] by increasing the effective surface area of the microelectrode, thereby reducing its electrical impedance. The porosity of electroplated platinum black[17,18] is highly dependent upon the microelectrode array geometry and deposition parameters, such as charge density and plating time.

Several papers concerning theory and simulation of microelectrode array behavior have been published in recent years[3,14,19,20] together with some experimental investigations.[21] However, to our knowledge, an electrochemical study involving the systematic variation of *r* and *d*/*r* has not been reported. To complement and extend the existing literature, we investigated the electrochemical behavior of a system of microfabricated electrode arrays. Two sets of arrays were studied by cyclic voltammetry and chronoamperometry, one with the same relative center−center spacing and another with the same individual electrode diameter. Variation in electrode porosity was also explored by electroplating the microelectrode arrays with platinum black. Peak and steady-state current densities and signal-to-noise ratios (SNR) were obtained for the microelectrode arrays, and the results were considered in relation to microelectrode theory and their application to the design of an electrochemical sensor. Finally, a microelectrode array-based sensor was employed for the mediated enzymatic detection of hydrogen peroxide and the response time of different microelectrode array geometries was compared.

EXPERIMENTAL SECTION

Materials. Si_3N_4-coated, n-type Si(100) wafers were obtained from Edinburgh Microfabrication Facility (Edinburgh, U.K.), Shipley S1818 photoresist was from Chestech Ltd. (Warwickshire, U.K.), and silicone 3140 RTV coating was from Dow Corning (Coventry, U.K.). For all electrochemical experiments, aside from those involving the hydrogen peroxide microsensor, a platinum coil auxiliary electrode and a Ag|AgCl reference electrode from Bioanalytical Systems (Cheshire, U.K.) were employed and all reagents, for both microfabrication and electrochemical experiments, were purchased from Sigma-Aldrich (Poole, U.K.).

Microfabrication. Arrays of microdisk electrodes were fabricated by standard photolithographic and reactive-ion etching (RIE) techniques. A 380-μm-thick Si(100) wafer, coated on both sides with 200 nm of Si_3N_4, was employed as the substrate. 10 nm of Ti, 10 nm of Pd, and 100 nm of Au were deposited onto the substrate by electron beam evaporation, the Ti functioning as an adhesive layer[22] and the Pd preventing Ti diffusion along the Au grain boundaries.[23] A photoresist mask was patterned over the metal film to define the cathode, connecting wire, and bonding pad. The Ti/Pd/Au layer was then wet etched in 0.7 M HF and 1 M KI/0.2 M I_2 solutions. After removing the photoresist mask with acetone, the wafer was cleaned in an oxygen plasma (5 min

(13) Wittstock, G.; Grundig, B.; Strehlitz, B.; Zimmer, K. *Electroanalysis* **1998**, *10* (8), 526−531.
(14) Lee, H. J.; Beriet, C.; Ferrigno, R.; Girault, H. H. *J. Electroanal. Chem.* **2001**, *502* (1−2), 138−145.
(15) Zhu, H. X.; Lo, T. C.; Lenigk, R.; Renneberg, R. *Sens. Actuators, B* **1998**, *46*, 155−159.
(16) Elliott, J. M.; Birkin, P. R.; Bartlett, P. N.; Attard, G. S. *Langmuir* **1999**, *15*, (22), 7411−7415.
(17) Birkin, P. R.; Elliott J. M.; Watson, Y. E. *Chem. Commun.* **2000**, *17*, 1693−1694.
(18) Layson, A. R.; Columbia, M. R. *Microchem. J.* **1997**, *56* (1), 103−113.
(19) Beriet, C.; Ferrigno, R.; Girault, H. H. *J. Electroanal. Chem.* **2000**, *486* (1), 56−64.
(20) Morf, W. E. *Anal. Chim. Acta* **1997**, *341* (2−3), 121−127.
(21) Kudera, M.; Hill, H. A. O.; Dobson, P. J.; Leigh, P. A.; McIntire, W. S. *Sensors* **2001**, *1*, 18−28.
(22) Vogt, K. W.; Kohl, P. A.; Carter, W. B.; Bell R. A.; Bottomley, L. A. *Surf. Sci.* **1994**, *301*, 203−213.
(23) Sharp, D. J. *J. Vac. Sci. Technol.* **1979**, *16* (2), 204−207.

Table 1. Overview of the Microelectrode Array Geometries Investigated

set A: individual electrode diameter (μm)	no. of electrodes in array	total area of array (10^{-9} m^2)
100.0	4	31.4
50.0	9	17.7
25.0	25	12.3
10.0	121	9.5
5.0	441	8.7
2.5	1681	8.3
set B: *d*/*r* ratio	**no. of electrodes in array**	**total area of array (10^{-9} m^2)**
150	9	0.18
30	121	2.4
12	676	13.3
6	2601	51.1

[a] Set A microelectrode arrays have a constant *d*/*r* of 10, while set B arrays have a constant individual electrode diameter of 5 μm.

Table 2. Optimized Parameters for the Controlled Electrodeposition of Platinum Black onto the Microelectrode Arrays

individual electrode diameter (μm)	plating time (s)	applied current (μA)
100.0	180	10
50.0	150	11
25.0	120	13
10.0	90	15
5.0	75	18
2.5	60	20

at 70 W, 30 mT, and 2 L/min oxygen) using a Plasmafab 505 Barrel Asher (Electrotech, London). This produced a sufficiently clean surface for deposition of the insulation layer. A 500-nm Si_3N_4 layer was then deposited by plasma-enhanced chemical vapor deposition (PECVD) using an Oxford Plasma Technology 80 Plus system (Plasmatech, Bristol, U.K.). To promote the adhesion and robustness of this insulation layer, a low-stress PECVD method was employed.[24] A second photoresist mask was then spun over the Si_3N_4 and patterned to produce an array of microholes above the Si_3N_4-covered metal cathode. Therefore, when the sample was etched in a C_2F_6 plasma (12 min at 100 W, 15 mT, and 20 mL/min C_2F_6) with a Oxford Plasma Technology BP80 system (Plasmatech), the exposed areas of Si_3N_4 were removed, producing a high-aspect ratio, parallel array of recessed microelectrodes. The photoresist mask was then removed in acetone. Finally, the wafer was diced, connecting wires were soldered to the individual devices, and the solder joints were insulated with a silicone rubber.

For the enzyme-linked electrochemical assay of hydrogen peroxide, a microsensor incorporating a gold counter electrode (19 mm^2) and a Ag|Ag_3PO_4 (2 mm^2) reference electrode was fabricated. To remove uncertainties due to variation in microreference and solution composition when the response of microelectrode arrays with different center−center spacings was compared, a substrate was fabricated that supported six individually addressable working electrodes, with the counter electrode surrounding all six. Five of these were microelectrode arrays with varying center−center spacings, and the sixth was a single electrode with no overlying insulation layer. The microsenor was fabricated using the lithographic techniques described previously, and the procedure for the electrodepostion of Ag|Ag_3PO_4 is described below.

Microelectrode Arrays with Constant *d*/*r*. A range of rectangular microelectrode arrays were fabricated such that the center-to-center distance of the electrodes in the outermost rows, *l*, was 500 μm, the center-to-center distance between adjacent microelectrodes being 10*r* (set A, described in Table 1). To ensure a high yield of fully functional devices, the smallest microelectrodes employed had a diameter of 2.5 μm, which is slightly larger than the practical minimum feature size of a laboratory-based photolithography system.

Microelectrode Arrays with Constant *r*. The second set of microelectrode arrays investigated had varying center-to-center spacings and a constant individual electrode diameter of 5 μm. The center-to-center distance of the electrodes in the outermost rows was 750 μm (set B, described in Table 1).

Microsensor For Bioanalytical Measurements. Five different working microelectrode arrays were investigated, the individual electrode diameter of each array being 10 μm. The relative center−center spacings employed were 4, 6, 10, 18, and 34, and the arrays were patterned within a 1-mm^2 area.

Electrodepostion. In addition to the thin-film gold microelectrode arrays, platinum black arrays were also investigated. Prior to electroplating, the arrays were cleaned in an oxygen plasma for 60 s (operating conditions as noted previously) to remove any passivating materials, as reported by Cai et al.[25] Platinum black was electroplated from a solution containing 24 mM hydrogen hexachloroplatinate and 2.1 mM lead acetate by both chronoamperometry and chronopotentiometry. The deposition was performed using an EG&G 273A potentiostat−galvanostat controlled by a PC with associated electrochemistry software (EG&G Princeton Applied Research). For chronopotentiometry, the optimum current and plating time, neither of which scaled linearly with area, were determined empirically for each set A device and are detailed in Table 2. Ag|Ag_3PO_4 was electroplated similarly. First a Ag layer was deposited using a 0.2 M silver nitrate/2.0 M potassium iodide/0.5 mM sodium thiosulfate solution with a current of 10 μA for 300 s. The electrode was then repeatedly cycled (−0.2 to +0.2 V versus Ag/AgCl at a scan rate of 5 mV/s) in a 0.1 M H_3PO_4 solution to form the Ag_3PO_4 layer. During the final cycle, the electrodes were disconnected part way through, after half the charge of a full cycle had passed.

Electrochemical Recordings. All microelectrode array experiments were performed within a Faraday cage and employed a three-electrode cell, with a platinum coil auxiliary electrode and a Ag|AgCl reference electrode. A CV-37 potentiostat (BAS Instruments Ltd., Cheshire, U.K.), a PC26AT data acquisition card (Amplicon Liveline Ltd., Brighton, U.K.), and an in-house data-handling program were employed to record the electrochemical signals. The laboratory temperature was 24 ± 1 °C.

Again, prior to all electrochemical measurements, the devices were cleaned in an oxygen plasma for 60 s (operating conditions

(24) French, P. J.; Sarro, P. M.; Mallee, R.; Fakkeldij, E. J. M.; Wolffenbuttel, R. F. *Sens. Actuators, A-Phys.* **1997**, *58*, 149−157.

(25) Cai, X.; Klauke, N.; Glidle, A.; Cobbold, P.; Smith, G. L.; Cooper, J. M. *Anal. Chem.* **2002**, *74* (4), 908−914.

as noted previously). Cyclic voltammograms (10 mV/s) were recorded for each gold microelectrode array in a 1 mM ferrocenemonocarboxylic acid (FMCA)/10 mM phosphate-buffered saline (PBS) solution and linear sweep voltammograms (20 mV/s) in oxygen-saturated water. Background voltammograms were recorded in 10 mM PBS and a saturated Na_2SO_3 solution (Na_2SO_3 being an effective oxygen scavenger) that had been completely deoxygenated by bubbling nitrogen through the solution for 10 min prior to recording. Recordings were made in triplicate, and all calculations employed mean values.

To optimize the performance of a microelectrode array sensor in an aqueous environment, chronoamperometric measurements were then acquired for both gold and platinum black arrays in water that had been equilibrated to room temperature and oxygen level for several hours. To allow the output signal to fully stabilize, the gold microelectrode arrays were polarized at −0.7 V versus Ag|AgCl for 10 min prior to recording while the platinum black arrays were polarized for 15 min. Background recordings were obtained as before, and calculations resulting from the chronoamperometric recordings employed time-averaged values. Noise was defined as 3 standard deviations of the recorded signal.

Bioanalytical Measurements. For the enzyme-linked electrochemical assay of H_2O_2, aliquots ranging from 10 to 200 μL of 9 mM H_2O_2 in 0.2 M phosphate buffer solution (pH 7) were added to 1 mL of a 0.2 M phosphate buffer solution containing 0.1 mg of type I horseradish peroxidase (HRP) and 2 mM ferrocenemethanol (FcOH). Before being added to the phosphate buffer, the FcOH was dissolved in 100 μL of methanol. Immediately after the addition of the H_2O_2 aliquot, the solution was mixed for 15 s using a vortex mixer and was then injected into an electrochemical cell containing the microelectrode array within a further 15 s. A potential of 0 V (vs Ag/Ag_3PO_4) was applied to detect the oxidized FcOH, which was acting as a mediator for horseradish peroxidase. Chronoamperometric measurements were also made in a 1 mM FcOH/0.1 M $NaClO_4$ solution.

RESULTS AND DISCUSSION

Microelectrode Array Durability. A low-stress PECVD procedure was employed to improve the adhesion of the Si_3N_4 layer to the underlying metal film. Microelectrode arrays fabricated using standard PECVD Si_3N_4 had proved unsatisfactory for electrochemical experiments, as the adhesion of this Si_3N_4 to the underlying metal was poor, with fracturing and delamination of the Si_3N_4 layer frequently occurring, particularly at the edges of the microholes. However, employing a low-stress Si_3N_4 insulation layer greatly improved adhesion to the underlying metal film, and no delamination or breakdown of the dielectric was observed. The microelectrode arrays (Figure 1) were extremely durable, and by oxygen cleaning the devices prior to each experiment, they proved effective for repeated electrochemical trials.

Voltammetry. To investigate the electrochemical behavior of the microelectrode arrays, cyclic voltammograms were first recorded for a model electroactive species, FMCA. Typical voltammograms for the Au arrays of set A are presented in Figure 2a. As the individual microelectrode diameter was increased from 2.5 to 50 μm, the recorded oxidation peak current, I_{pk}, decreased, while I_{pk} for the 100−μm array was slightly larger than that of the 50-μm array. As r is increased, the active area of the microelectrode array becomes larger. For a finite microelectrode

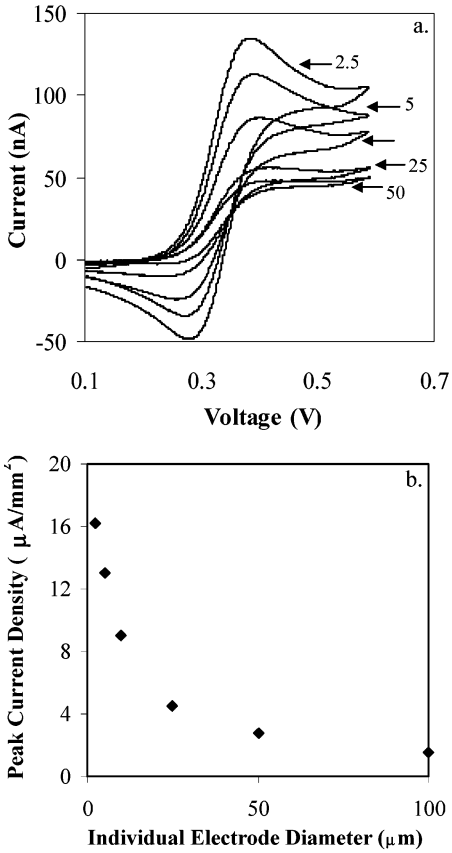

Figure 2. (a) Typical cyclic voltammograms recorded in 1 mM FMCA (10 mV/s) with the set A microelectrode arrays. The individual electrode diameter (μm) of the corresponding array is marked for each voltammogram. For clarity, the voltammogram generated by the 100−μm electrode array is not shown. (b) The mean peak current densities obtained from the above voltammograms.

Table 3. Average Current and Current Density Values at −0.7 V vs Ag|AgCl from Linear Sweep Voltammograms Recorded in a Saturated Oxygen Solution at 24 ± 1 °C

individual electrode diameter (μm)	current (nA)	current density (μA/mm^2)
100.0	−130	−4.1
50.0	−115	−6.5
25.0	−124	−10.1
10.0	−150	−15.8
5.0	−181	−20.9
2.5	−235	−28.5

array, the active area can be expressed as $\pi(r + a)^2$, where $a = l/(d/r)$. Therefore, the greatest increase in active area was between the 50−μm array and the 100-μm array, which explains why a larger I_{pk} was generated by the latter when compared to the former. This overall trend in I_{pk} variation with individual microelectrode diameter was observed repeatedly over a number of experiments, including the recording of linear sweep voltammograms (from 0 to −0.7 V vs Ag|AgCl) in a saturated oxygen solution (Table 3).

From the FMCA voltammograms, the average peak current densities were calculated for each microelectrode array (Figure 2b) to normalize the data with respect to the cumulative area of the individual microelectrodes. As expected, the 2.5-μm array generated the largest current density, 10 times greater than the

Table 4. Mean Peak−Peak Separation and Peak Strength Values for the Microelectrode Arrays Investigated Obtained from Cyclic Voltammograms Recorded in 1 mM FMCA

set A: individual electrode diameter (μm)	peak−peak separation (mV)	peak strength (10^{-9} m^2)
25.0	193	−27
10.0	145	−82
5.0	119	−168
2.5	106	−256
set B: d/r ratio	**peak−peak separation (mV)**	**peak strength (10^{-9} m^2)**
30	246	−18
12	135	−279
6	97	−700

smallest current density, which was produced by the 100−μm array.

It can be seen from Figure 2a that the shape of each voltammogram is strongly dependent upon the individual microelectrode diameter. The 2.5−μm array produced a strongly peak-shaped curve, which indicates a quasi-reversible linear diffusion to the electroactive sites. As the individual electrode diameter increased, the microelectrode arrays generated current−potential curves with increasingly smaller peaks, the 50-μm array producing an essentially sigmoidal curve.

The peak−peak (E_{pk-pk}) separation for the voltammograms produced by the 2.5-, 5-, 10-, and 25-μm arrays (the arrays that generated peaked curves of varying degrees) increased with r, while the strength of the oxidation peak decreased (Table 4) and the reductive wave diminished. Peak strength was defined as the average gradient of the curve for potential range $E_{pk} < E < (E_{pk} + 80$ mV$)$, that is, the average gradient for the region of the voltammograms where a macroelectrode would generate a current that decreases sharply from I_{pk}. As a sigmoidal voltammogram, which has no peaks, is produced when diffusion to a microelectrode array is radial, the measured peak strength of the arrays should tend toward zero as diffusion becomes increasingly radial. Therefore, peak strength variation may be used in a semiquantitative manner to estimate the smallest individual electrode diameter for which radial diffusion alone will be observed. In this case ($d/r = 10$), as the measured peak strength tends toward zero, the individual electrode diameter tends toward 50 μm, for which sigmoidal behavior was indeed observed.

The diffusion profile of an electroactive species toward an array of microelectrodes may be one of the following: hemispherical, when the individual microelectrodes operate independently of each other; linear, when the diffusion fields of the individual microelectrodes merge completely; or mixed, when the individual diffusion layers partially merge. The cyclic voltammograms obtained demonstrate how, for a constant center-to-center spacing, the degree to which the diffusion layers merge is dependent upon the diameter of the individual microelectrodes. While the arrays of larger microelectrodes exhibited radial diffusion behavior, the diffusion fields of the smaller microelectrodes (with a diameter of <10 μm) appeared to merge considerably, resulting in a peaked voltammogram indicative of linear diffusion.

This trend can be explained in part by the so-called edge effect that is displayed by finite arrays of densely packed microelectrodes.[14] The current density generated by microelectrodes at the perimeter of such an array will be noticeably larger than that generated by those in the center, due to the radial nature of diffusion toward the outer areas of the perimeter electrodes.[19] For the same geometric area and d/r value, arrays of large microelectrodes will have a greater perimeter-to-internal electrode ratio when compared to arrays of smaller microelectrodes; hence, the nonlinearity of diffusion to the former will be greater. Similarly, for the same individual electrode diameter and d/r value, arrays with a smaller geometric area will have a greater perimeter-to-internal electrode ratio when compared to arrays of larger areas. Furthermore, relative to the circumference of the individual microelectrodes, the inactive area surrounding each electrode decreases significantly with the radius. Therefore, despite a greater circumference-to-surface area ratio, which promotes radial diffusion, arrays of smaller microelectrodes will not exhibit as nonlinear a diffusion profile as arrays of larger microelectrodes, as there is not as comparatively large an inactive area surrounding them. Consequently, to ensure electrochemical behavior that retains microelectrode characteristics, as the diameter of the individual electrodes of an array decreases, the d/r value must be increased.

As classical microelectrode behavior was not demonstrated by the microelectrode arrays with smaller individual electrodes, a second set of arrays (set B), with a constant individual electrode diameter of 5 μm was investigated. Typical cyclic voltammograms obtained from the arrays in FMCA solution are presented in Figure 3a. As expected, the electrochemical behavior of the microelectrode arrays varied significantly with d/r. A strongly peaked voltammogram was produced by the array with a d/r of 6, while the array with a d/r of 150 produced a sigmoidal curve, indicative of radial diffusion. The intermediary microelectrode arrays produced cyclic voltammograms with mixed diffusion characteristics.

The peak−peak separation and the peak strength obtained for the arrays with a d/r of 6, 12, and 30 are presented in Table 4. An increase in the center-to-center spacing resulted in an increase in the peak−peak separation, a decrease in the peak strength, and an increase in the current density (Figure 3b), due to the enhanced nonlinearity of the diffusion profile. From the decreasing peak strength values, it can be estimated that a minimum center-to-center spacing of approximately $d/r = 40$ is required to ensure fully hemispherical diffusion to microelectrode arrays with an individual electrode diameter of 5 μm.

Chronoamperometric Measurements. Chronoamperometric measurements were obtained for each microelectrode array in set A, before and after platinization. It should be noted that the platinum black arrays were polarized for a longer period prior to recording as they did not stabilize as quickly as the gold arrays.

Variation in current density with r was similar to that observed previously, and the current densities generated by the platinum black microelectrode arrays (calculated using the active area prior to electrodeposition rather than the effective surface area) were consistently larger than those generated by the gold microelectrode arrays (Figure 4a). A comparison of experimental and theoretical currents, calculated for each gold microelectrode array

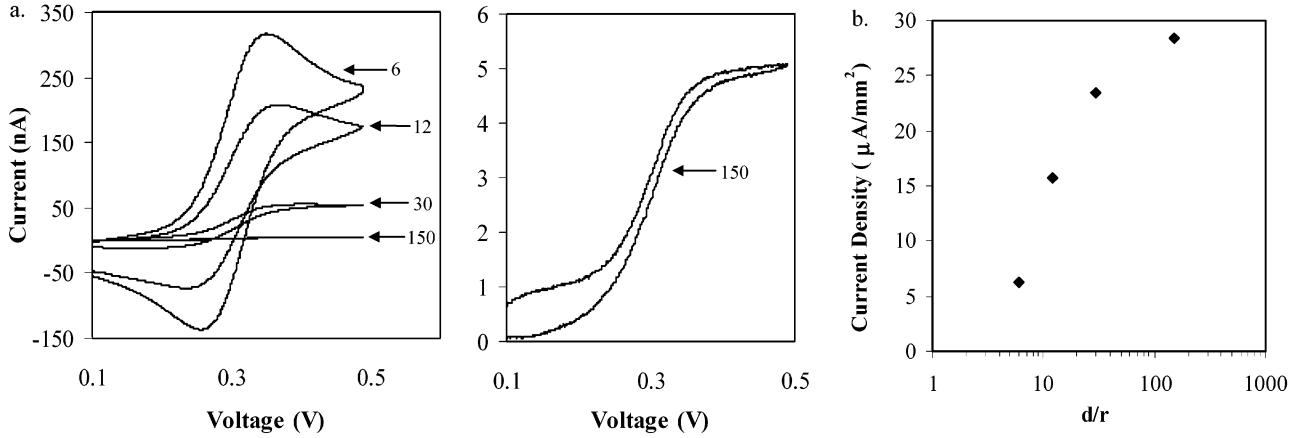

Figure 3. (a) Typical cyclic voltammograms recorded in 1 mM FMCA (10 mV/s) with the set B microelectrode arrays. The *d*/*r* ratio of the corresponding array is marked for each voltammogram, and an expanded view of the graph produced by the microelectrode array with a *d*/*r* ratio of 150 is also shown. (b) The mean peak current densities obtained from the above voltammograms.

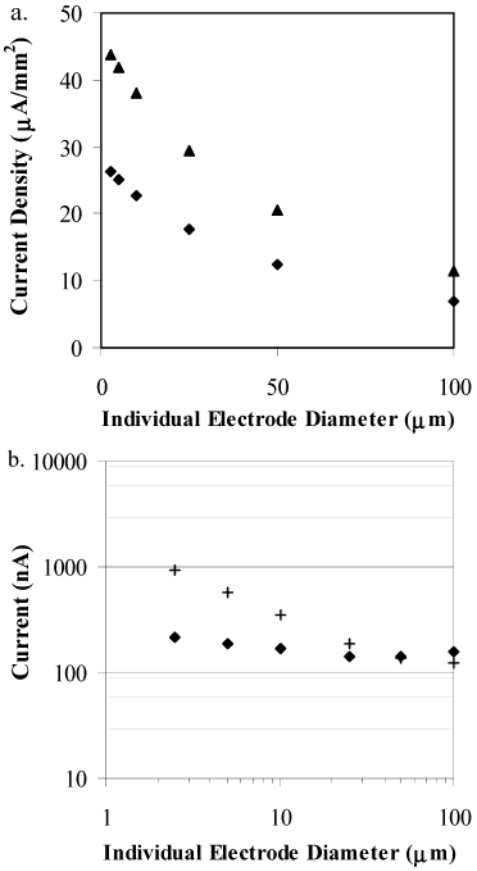

Figure 4. (a) Time-averaged current densities from dissolved-oxygen current−time recordings (−0.7 V) for gold (◆) and platinum black (▲) set A microelectrode arrays. (b) Comparison of theoretical (+) and experimental (◆) currents for above current−time recordings.

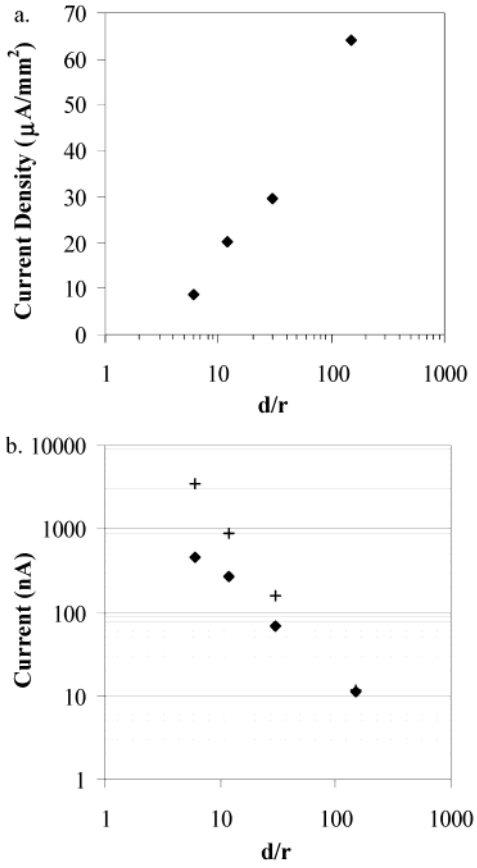

Figure 5. (a) Time-averaged current densities from dissolved-oxygen current−time recordings (−0.7 V) using set B microelectrode arrays. (b) Comparison of theoretical (+) and experimental (◆) currents for above current−time recordings.

using eq 1 for *m* microelectrodes, is shown in Figure 4b. It can be seen that the arrays with the largest individual electrodes did generate a current similar to the theoretical value for an array of microelectrodes exhibiting nonlinear diffusion. However, as the individual electrode diameter is decreased, the observed current becomes significantly smaller than that predicted by eq 1. This confirms that, for microelectrode arrays with the same *d*/*r*, the smaller the individual microelectrode, the greater the linear component of the mixed diffusion profile.

Current−time recordings were also obtained for each microelectrode array in set B, although Au arrays alone were investigated. Variation in the recorded current density with *d*/*r* (Figure 5a) was similar to that obtained previously. A comparison of experimental and theoretical currents is presented in Figure 5b, the theoretical values again calculated from eq 1 for *m* microelectrodes. The theoretical and experimental currents for a *d*/*r* of 150 are comparable, verifying that the diffusion profile of the electroactive species is indeed radial. However, as *d*/*r* decreases,

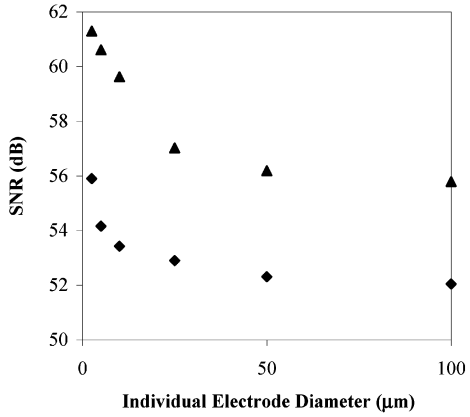

Figure 6. SNRs for gold (◆) and platinum black (▲) set A microelectrode arrays calculated from dissolved oxygen current−time recordings (Figure 4a).

the experimental currents progressively deviate from the theoretical values, confirming the increased linearity of diffusion to microelectrode arrays with smaller center-to-center spacings.

For all set A microelectrode arrays, the SNR for the system employed was determined (Figure 6), the SNR being expressed in decibels:

$$\mathrm{SNR} = 20 \log(\mathrm{signal}/\mathrm{noise}) \qquad (2)$$

A signal/background ratio (SBR) may be expressed similarly, but whereas noise was defined as three standard deviations of the recorded signal and was mainly due to electrical instrumentation noise, background was simply defined as the time-averaged current recorded in an analyte-free solution. Variation with individual microelectrode diameter again demonstrated a trend similar to that observed previously, with the smallest electrodes producing the largest SNRs and platinum black microelectrode arrays producing larger SNRs than gold microelectrode arrays. However, the average background current for the platinum black arrays (−0.44 nA) was noticeably larger than that for the gold arrays (−0.21 nA), due to the greatly increased surface area. Therefore, electroplating with platinum black decreased the SBR but increased the SNR, which would produce an overall increase in the resolution of an amperometric sensor employing a microelectrode array.

Morphology of Platinum Black Electrode Arrays. A comparison of the gold and platinum black microelectrode array signals requires some consideration of the morphology of the electroplated films (Figure 7). The electrode diameter of the largest microelectrodes was not significantly altered by electroplating platinum black, as any growth outward over the Si_3N_4 layer was not significant when compared to the microelectrode size. However, if the plating current was not carefully controlled, the smallest gold electrodes frequently more than doubled in size during electroplating and became hemispherical in shape and highly porous. Furthermore, it should be noted that those microelectrodes on the outside of the arrays were the most overplated due to the edge effect that was discussed previously.

Rigorous attempts were therefore made to produce a constant electrode morphology and to control the individual electrode diameter and porosity, as this study required comparable microelectrode arrays. However, even with careful control of the electroplating process, some outward plating was unavoidable. When plating electrodes of lower porosity, by decreasing the deposition rate, only slight overplating and minimal d/r variation occurred (Figure 7a). The most favorable electrodeposition parameters for this study were given previously, chronopotentiometry being the most readily controllable method of deposition.

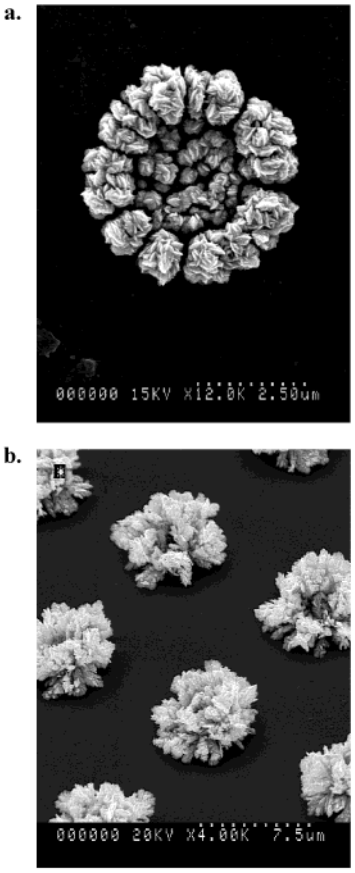

Figure 7. (a) A 5-μm platinum black electrode, electroplated at a low deposition rate to ensure minimal overplating; (b) extremely porous, hemispherical, platinum black electrodes (~6-μm diameter), electroplated through a 2.5-μm-diameter hole.

Although the platinum black microelectrode arrays did generate noticeably larger signals than the gold arrays, the increase was not as large as may be expected due to the low electrodeposition rates that had to be employed. Furthermore, the data acquired for the microelectrode arrays with the smallest individual electrodes should be considered in light of the unavoidable but slight increase in area during electroplating. If highly porous platinum black electrodes are to be deposited, compensation for the inevitable increase in electrode diameter is required when an insulation layer is designed for a specific electrode diameter and interelectrode spacing. With an array of such electrodes, the current obtained was typically enhanced by a factor of ~6 when compared to an array of evaporated gold electrodes. For example, an array of highly porous microelectrodes that were virtually hemispherical in shape was electrodeposited (as shown in Figure 7b) and produced a 6.5-fold increase in the output signal.

When an electrochemical sensor is designed that incorporates a microelectrode array, the optimum geometry of the array will

depend on the proposed application and operation of the sensor. For voltammetric microsensors, radial diffusion is highly advantageous, as it permits the acquisition of steady-state measurements and the use of very fast scan rates. Furthermore, if a flow-independent sensor is desirable, radial diffusion will minimize the convection dependence of the sensor. In situations where radial diffusion is desirable, it has been demonstrated that the smaller the individual electrodes of an array, the greater the interelectrode spacing required. For a steady-state amperometric sensor, a high SNR is generally the main concern. Small individual microelectrodes with small center-to-center spacings have been shown to produce large SNRs, with the electrodeposition of platinum black increasing the SNR further. However, if very fast response times are required for such a sensor, larger center-to-center spacings may be preferential, as this will increase the nonlinearity of the diffusion profile and therefore the time taken to reach a steady state will be greatly reduced.

Bioanalytical Measurements. To illustrate the improved response time obtained with arrays that have an increased center−center spacing, the microelectrode sensor was used to measure the current−time transients during the oxidation of FcOH (as a model system) and then, subsequently, during the horseradish peroxidase-catalyzed oxidation of hydrogen peroxide in the presence of FcOH.

To allow comparison of the temporal response of the various working microelectrode arrays, the current−time responses (Figure 8a) were normalized using the current measured at 1000 s. It can be seen that the current transient for the single large electrode, which exhibits the expected $t^{-1/2}$-dependent Cottrell behavior, varies significantly during the recording period. The response of the sparsely spaced microelectrode arrays, however, tends toward a steady state more quickly. A flatter current response is advantageous when an assay protocol is used in which data are collected over a limited period of time or when it is necessary to decouple the temporal electrochemical response from solution kinetics (e.g., in an enzyme mediated reaction).

A quantitative comparison of the time-dependent response of the oxidation of FcOH can be made by measuring the time taken for the current to reach either 10% or 20% of the value recorded at either 300 or 600 s. This is tabulated in Table 5 and shows that, whereas it is necessary to wait 390 s for the current at the single electrode to come within 10% of the 600-s value, for the microelectrode arrays with a d/r value of greater than 10, it is only necessary to wait 180 s.

A similar trend was observed for the mediated enzyme-linked assay for hydrogen peroxide. Figure 8b shows the current corresponding to the reduction of ferrocenemethanol, following the injection of the solution containing H_2O_2. The uniformity of the step increases in current (when using a log scale) shows that a doubling in the concentration of H_2O_2 leads to a doubling in the measured current for all electrodes; i.e., concentration is linear with the current response. A comparison of the response time for the single electrode and for the microelectrode arrays is also readily made using a log-scale plot. These results are quantified in Table 5 and show that a good estimate of the steady-state current may be made after ~20 s when a microelectrode array with a d/r value of 34 is used. Furthermore, it was observed from the data in Figure 8 that loosely packed microelectrode arrays

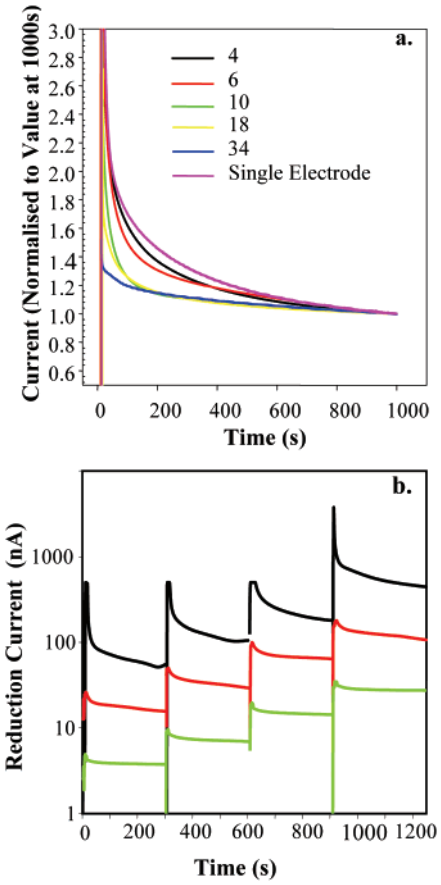

Figure 8. (a) Current−time transients for the electrode arrays in 1 mM FcOH solution using the microelectrode array sensor. The key indicates the relative center−center spacing for each trace. (b) Log of the reduction current recorded for an enzyme-linked assay (described in detail in the text) after injection of solutions containing 10-, 20-, 40-, and 80-μL aliquots of 9 mM H_2O_2, respectively, for the single working electrode (black trace) and the working microelectrode array with a d/r value of 10 (red) and of 34 (green).

Table 5. Time (s) Taken for the Microsensor To Reach Both 80% (t_{80}) and 90% (t_{90}) of the Value at 300 and 600 s for Both the FcOH Recordings and the Mediated Enzyme-Linked H_2O_2 Assay

	oxidation of FcOH				H_2O_2 assay	
d/r value	t_{80} (300 s)	t_{90} (300 s)	t_{80} (600 s)	t_{90} (600 s)	t_{80} (300 s)	t_{90} (300 s)
single electrode	120	200	300	390	140	220
4	120	195	230	320	100	200
6	100	160	180	280	85	140
10	60	100	90	180	55	100
18	40	100	90	180	20	90
34	20	60	50	180	20	65

generated a smoother signal than densely packed arrays or the large single electrode, due to a decreased sensitivity to convection influences, which is a characteristic of microelectrode behavior.

The fast electrochemical response obtained with such "loosely packed" microelectrode array-based sensor may be useful in the design of a variety of biosensors, for example, in the implementation of a heterogeneous electrochemical ELISA, where HRP is often used as an enzyme label.[26]

CONCLUSION

A range of microelectrode arrays with varying individual electrode diameters and center-to-center spacings has been systematically investigated. For $d/r = 10$, microelectrode arrays with an individual electrode diameter of 50 and 100 μm demonstrated sigmoidal behavior. However, as r decreased, the recorded voltammograms became increasingly peak-shaped, due to the increased linearity of the diffusion fields. Nonetheless, the peak current densities were the largest for the microelectrode arrays with the smallest individual electrodes. To achieve radial diffusion to a microelectrode array with an individual electrode diameter of 5 μm, an approximate center-to-center spacing of $d/r = 40$ was required. As expected from simulation work in the literature, loosely packed arrays produced significantly higher current densities than arrays with small center-to-center spacings, due to the merging of individual diffusion fields in the later case. A mediated enzyme-linked hydrogen peroxide assay, employing working microelectrode arrays of different center−center spacings, also showed an improved temporal response, in tending toward a steady state, for arrays with large d/r ratios.

Electroplating microelectrode arrays with platinum black increased the recorded currents and the SNRs, though the morphology and resulting diameter of highly porous platinum black electrodes proved difficult to accurately control. Electroplating highly porous platinum black onto the microelectrode arrays increased the recorded current by 6.5-fold.

(26) Niwa, O.; Xu, Y.; Halsall, H. B.; Heineman, W. R.; *Anal. Chem.* **1993**, *65* (11), 1559−1563.

ACKNOWLEDGMENT

The authors thank Dr. XinXia Cai for helpful discussions on electrode regeneration and electrodepostion. This work was supported by EPSRC, Kodak Analytical Services, Unilever, and E.U. project BRPR-CT97-0502.

Received for review March 25, 2002. Revised manuscript received August 7, 2002. Accepted September 4, 2002.

AC025649W